Lateral Variations of Interplate Coupling along the Mexican Subduction Interface: Relationships with Long-Term Morphology and Fault Zone Mechanical Properties

Baptiste Rousset,[1] Cécile Lasserre,[1] Nadaya Cubas,[2] Shannon Graham,[3] Mathilde Radiguet,[1] Charles DeMets,[4] Anne Socquet,[1] Michel Campillo,[1] Vladimir Kostoglodov,[5] Enrique Cabral-Cano,[5] Nathalie Cotte,[1] and Andrea Walpersdorf[1]

Abstract—Although patterns of interseismic strain accumulation above subduction zones are now routinely characterised using geodetic measurements, their physical origin, persistency through time, and relationships to seismic hazard and long-term deformation are still debated. Here, we use GPS and morphological observations from southern Mexico to explore potential mechanical links between variations in inter-SSE (in between slow slip events) coupling along the Mexico subduction zone and the long-term topography of the coastal regions from Guerrero to Oaxaca. Inter-SSE coupling solutions for two different geometries of the subduction interface are derived from an inversion of continuous GPS time series corrected from slow slip events. They reveal strong along-strike variations in the shallow coupling (i.e. at depths down to 25 km), with high-coupling zones (coupling >0.7) alternating with low-coupling zones (coupling <0.3). Coupling below the continent is typically strong (>0.7) and transitions to uncoupled, steady slip at a relatively uniform ~175-km inland from the trench. Along-strike variations in the coast-to-trench distances are strongly correlated with the GPS-derived forearc coupling variations. To explore a mechanical explanation for this correlation, we apply Coulomb wedge theory, constrained by local topographic, bathymetric, and subducting-slab slopes. Critical state areas, i.e. areas where the inner subduction wedge deforms, are spatially correlated with transitions at shallow depth between uncoupled and coupled areas of the subduction interface. Two end-member models are considered to explain the correlation between coast-to-trench distances and along-strike variations in the inter-SSE coupling. The first postulates that the inter-SSE elastic strain is partitioned between slip along the subduction interface and homogeneous plastic permanent deformation of the upper plate. In the second, permanent plastic deformation is postulated to depend on frictional transitions along the subduction plate interface. Based on the location and friction values of the critical state areas identified by our Coulomb wedge analysis, we parameterise frictional transitions in plastic-static models of deformation over several seismic cycles. This predicts strong shear dissipation above frictional transitions on the subduction interface. The comparison of modelled surface displacements over a critical zone at a frictional transition and over a stable area with no internal wedge deformation shows differences of long-term uplift consistent with the observed along-strike variations in the coast-to-trench distances. Our work favours a model in which frictional asperities partly control short-term inter-SSE coupling as measured by geodesy and in which those asperities persist through time.

Key words: Middle America Trench, global positioning system, inter-SSE coupling, critical taper theory, plastic deformation, coastal morphology.

1. Introduction

Interseismic coupling maps derived from geodetic observations (e.g. Chlieh *et al.* 2014) are now widely used to represent 2D variations in strain along seismogenic zones and are providing increasingly detailed views of interseismic strain accumulation along major subduction zones (e.g. Mazzotti *et al.* 2000; Bürgmann *et al.* 2005; Franco *et al.* 2012; Nocquet *et al.* 2014). Although geodetic observations are now precise enough to distinguish fully coupled, locked sections of a fault from uncoupled or partially coupled sections, the physical origin, persistency through time, and hazard implications of geodetically derived coupling variations are still incompletely understood. Coupled areas appear to be roughly spatially correlated with rupture areas of

[1] ISTerre, CNRS, Univ. Grenoble Alpes, 38041 Grenoble, France. E-mail: baptiste.rousset@ujf-grenoble.fr

[2] Institut des Sciences de la Terre de Paris, Pierre et Marie Curie University, Paris, France.

[3] Department of Earth and Planetary Sciences, Harvard University, Cambridge, MA, USA.

[4] Department of Geoscience, University of Wisconsin-Madison, Madison, WI, USA.

[5] Instituto de Geofísica, Universidad Nacional Autónoma de México, CU, Coyoacan, Mexico.

major earthquakes, as shown for Mw8+ subduction earthquakes like in Sumatra (CHLIEH *et al.* 2008), Japan (LOVELESS and MEADE 2011) or the Andes (CHLIEH *et al.* 2011; METOIS *et al.* 2012). Along some subduction interfaces, areas that produce earthquakes, also called asperities, seem to be separated by areas of low coupling that may slow or arrest propagating rupture fronts. Large ruptures may break through such barriers (KONCA *et al.* 2008) due to dynamic effects (KANEKO *et al.* 2010; CUBAS *et al.* 2015). Most authors interpret variations in interseismic coupling, which may persist for a few decades or longer, as variations of frictional properties that may result from or influence other characteristics of a subduction zone such as its geology, morphology, and gravity, which may persist for millions of years. Features on the down-going plate such as seamounts or oceanic ridges may give rise to local variations in coupling along some subduction zones (e.g. SINGH *et al.* 2011), whereas morphological features of the overriding plate may control coupling variations elsewhere (BÉJAR-PIZARRO *et al.* 2013). A correlation between trench-parallel negative gravity anomalies and rupture areas of great earthquakes, as well as between positive gravity anomalies and aseismic creeping areas, is also observed (SONG and SIMONS 2003). All of these observations suggest that the seismogenic behaviour of subduction zones may be stationary over long time scales. Consistent with this idea, critical taper theory (DAHLEN 1984) postulates that the structure and morphology of a forearc prism depend on its mechanical properties, including its basal and internal friction angles and pore fluid pressure. Applied to subduction wedges in Chile and Japan (CUBAS *et al.* 2013a, b), this theory shows that parts of the wedge that are in a stable state are located above past earthquake rupture zones and strongly coupled areas of subduction interface, whereas areas that are at critical state (i.e. parts of the wedge that are affected by internal deformation) are associated with lower interseismic coupling and contour the stable areas.

In this study, we further explore the mechanical link between interseismic coupling, the characteristics of the slab interface and accretionary prism, and the long-term deformation of the overriding plate, possibly accumulated through non-elastic processes.

We focus on the Mexican subduction zone where the Cocos plate subducts below the North American plate. This area has been extensively studied from geodetic and seismological observations since the discovery of slow slip events (hereafter abbreviated "SSE") and tremors both in Guerrero and Oaxaca regions (e.g. LOWRY *et al.* 2001; BRUDZINSKI *et al.* 2007; CORREA-MORA *et al.* 2008, 2009; KOSTOGLODOV *et al.* 2010; WALPERSDORF *et al.* 2011; RADIGUET *et al.* 2012; HUSKER *et al.* 2012; GRAHAM *et al.* 2014a). To date, most studies of the spatio-temporal behaviour of slip along the Mexican subduction zone have focused separately on Guerrero and Oaxaca. With the increase of the GPS network density during the past years, especially in the Oaxaca region (GRAHAM *et al.* 2014b), a more regional analysis has become possible, as presented in this study.

Below, we use an interseismic GPS velocity field for southern Mexico measured in between SSE (inter-SSE velocity field) to retrieve a regional map of inter-SSE coupling from the Guerrero to the Oaxaca segments of the Mexico subduction zone. We first compute forward models to extract first order characteristics (downdip limit of coupling and data sensitivity to along-strike variations of coupling at shallow depth). We then invert for the 2D distribution of inter-SSE coupling on the subduction interface. We quantify along-strike variations in the shallow (depths of 0 to 25 km) coupling and compare them to along-strike variations in the coast-to-trench distances. Through a mechanical analysis of the long-term morphology of the accretionary wedge, following CUBAS *et al.* (2013a), we locate the critical state areas on the slab interface. This allows us to discuss, for the first time in this region, the persistency through time of inter-SSE coupling patterns and the mechanisms involved in the coastal long-term deformation of subduction zones.

2. Seismic and Aseismic Behaviour

Compared to other subduction zones, the Mexican subduction zone in the Guerrero-Oaxaca (Fig. 1) area has a narrow seismogenic zone, extending downdip by ~ 60 km (SUÁREZ and SÁNCHEZ 1996) to approximate depths of 25 km. Two areas devoid of
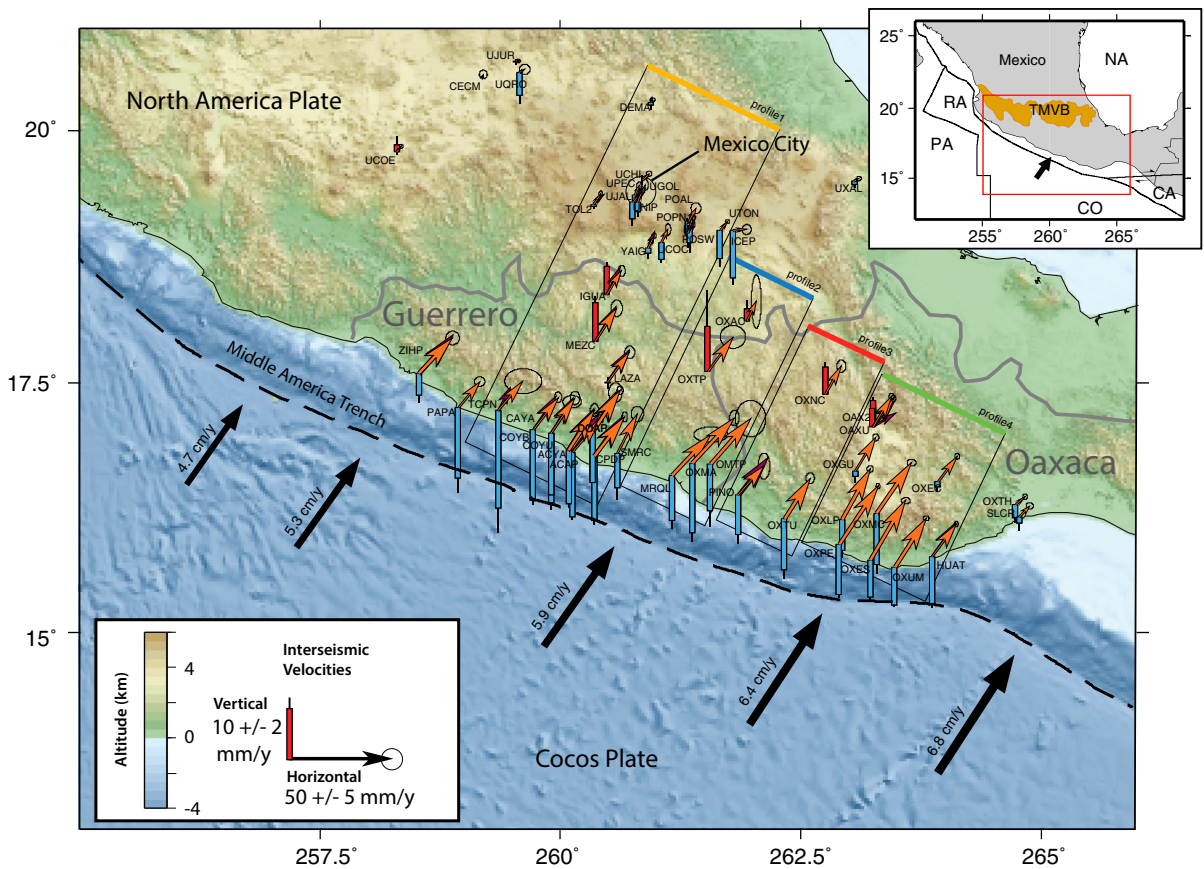
Figure 1
Inter-SSE GPS site velocities corrected for silent slip events as determined from GPS position time series. Velocities are relative to a stationary North America plate. *Orange* and *purple* vectors show horizontal velocities that are used in this study (54 stations) and by RADIGUET *et al.* (2012) (18 stations), respectively. Confidence ellipses $(1 - \sigma)$ are shown for this study only. *Vertical thick bars* show the vertical site rates used in this study (*blue* for subsidence and *red* for uplift). The *thin, vertical, black lines* indicate the $1 - \sigma$ uncertainty. The *black* vectors offshore show convergence velocities predicted by the PVEL Cocos–North America angular velocity (DEMETS *et al.* 2010). The four *black rectangles* with a coloured side delineate the groups of GPS stations that are used for our forward modelling. The topography and bathymetry are combined from SRTM (FARR *et al.* 2007) and ETOPO1 (AMANTE and EAKINS 2009) measurements. *Inset at top right corner* shows geodynamic setting, with convergence of Cocos (CO) towards North America (NA) plates. Adjacent plates are the Pacific (PA), the Riviera (RA) and the Caribbean (CA) plates. The Trans-Mexican Volcanic Belt (TMVB) is shown in *orange*

seismicity were defined as seismic gaps: the Michoacan and the Guerrero gaps (ASTIZ and KANAMORI 1984). The first was filled by the destructive M_w 8.1 Michoacan earthquake in 1985. The 200 km-long Guerrero Gap ruptured in 1957 and 1962 in its southeastern half (ORTIZ *et al.* 2000), while its remaining 100 km-long northwestern part has not broken since at least 1911 (KOSTOGLODOV *et al.* 1996).

Five SSEs have been detected in the Guerrero area since the installation of continuous GPS stations: in 1998, 2002, 2006, 2009 (LOWRY *et al.* 2001; KOSTOGLODOV *et al.* 2010; VERGNOLLE 2010; WALPERSDORF

et al. 2011; RADIGUET *et al.* 2011), and the most recent event in 2014. They recur approximately every 4 years (COTTE *et al.* 2009) and are among the largest SSEs in the world, with equivalent magnitudes of 7.5 (RADIGUET *et al.* 2012). Models of the 2006 event from GPS and InSAR data (RADIGUET *et al.* 2011; CAVALIÉ *et al.* 2013; BEKAERT *et al.* 2015) show that the SSE is located at the transition between the stick-slip and steady slip areas, with the SSE partly intruding updip into the seismogenic zone. From an analysis of 12 years of interseismic strain, RADIGUET *et al.* (2012) show that SSEs release about 75 % of

the elastic strain energy that is stored during the inter-SSE period. In the Oaxaca region, M_w 6.6–6.9 SSEs have been observed every 1–2 years since 1993, when continuous GPS measurements began there (Brudzinski et al. 2007; Marquez-Azua and DeMets 2009; Graham et al. 2014a). SSEs below Oaxaca do not appear to propagate updip into the seismogenic zone. Differences between Guerrero and Oaxaca regarding the location of the SSEs with respect to the potential seismogenic zone may be related to different phases of the seismic cycle for these two regions as suggested by seismic cycle modelling (e.g. Lapusta et al. 2000; Liu and Rice 2007). The 2011/2012 SSE below Oaxaca migrated ∼200 km along strike and may have triggered the 2012, M_w 7.2, Ometepec earthquake (Graham et al. 2014b).

Seismic tremors have also been detected both in Guerrero (Kostoglodov et al. 2010) and Oaxaca (Brudzinski et al. 2010). Although peak tremor activity below Guerrero is recorded during SSEs, smaller energy bursts are detected between major SSEs, possibly associated with smaller, barely detectable SSEs (Vergnolle 2010; Frank et al. 2015). Husker et al. (2012) describe two tremor sweet spots below southern Mexico, one at ∼215 km from the trench, downdip from the region populated by SSEs, where tremors are relatively continuous, and the other at 180–200 km from the trench, overlapping the SSE sweet spot and where tremor is more intermittent. Complementary studies of low frequency earthquakes (Frank et al. 2013) localise the low frequency events within the two tremor areas on the subduction interface, with a temporal behaviour similar to that of tremors and thrust focal mechanisms compatible with the subduction motion.

3. Analysis of Inter-SSE Coupling in Southern Mexico

3.1. GPS Data

Several continuous GPS networks are running in Mexico, operated by the Geophysical Institute (IG) and the National Seismological Service (SSN) of the National Autonomous University of Mexico (UNAM), and one GPS network by the Mexican National Institute of Statistics and Geography

(INEGI). Data presented in this paper cover the period 2005–2011, with a progressive densification of stations through time. Stations are mainly localised along the coast and along a profile going from Acapulco to Mexico City in the Guerrero region. In the Oaxaca region, stations are more sparse (Fig. 1). Extraction of the inter-SSE velocities, representing the strain accumulation between slow slip events, consists of fitting a site position time series via a linear regression that has been modified to also estimate and remove step functions due to earthquakes, slow slip events, and hardware changes and to mask periods when slow slip events occur. All continuous data employed for this study were processed using an identical methodology, which is fully described by Graham et al. (2014a, b). The best-fitting inter-SSE velocities relative to a stationary North America plate are plotted in Fig. 1 and are projected onto profiles in Fig. 2a, b. Horizontal velocities are maximal in the coastal area and decrease progressively. The site velocities are consistent with northeast-directed convergence of the Cocos plate with North America, as expected. The vertical rates show rapid subsidence along the littoral, a pattern that mimics the long-term morphology, which includes several large coastal lagoons. Inland, a band of present-day uplift at ∼125 km from the trench coincides with a high mountain range, the Sierra Madre del Sur. The inter-SSE vertical velocities taper to zero at ∼250 km from the trench. Compared to Radiguet et al. (2012), our study presents an increased number of GPS observations, and incorporates data from the Oaxaca region. At stations that are common to our studies, the GPS site velocities are consistent (compare orange and purple arrows on Fig. 1). We interpret this as evidence that the velocity estimates are robust given that different approaches were used in the two studies to extract the inter-SSE signal.

3.2. Forward Models

We begin with simple forward backslip modelling to approximate the downdip location of the transition between the coupled (or partially coupled) area and the deep, steady creeping area. We also test the sensitivity of the GPS velocities to along-strike
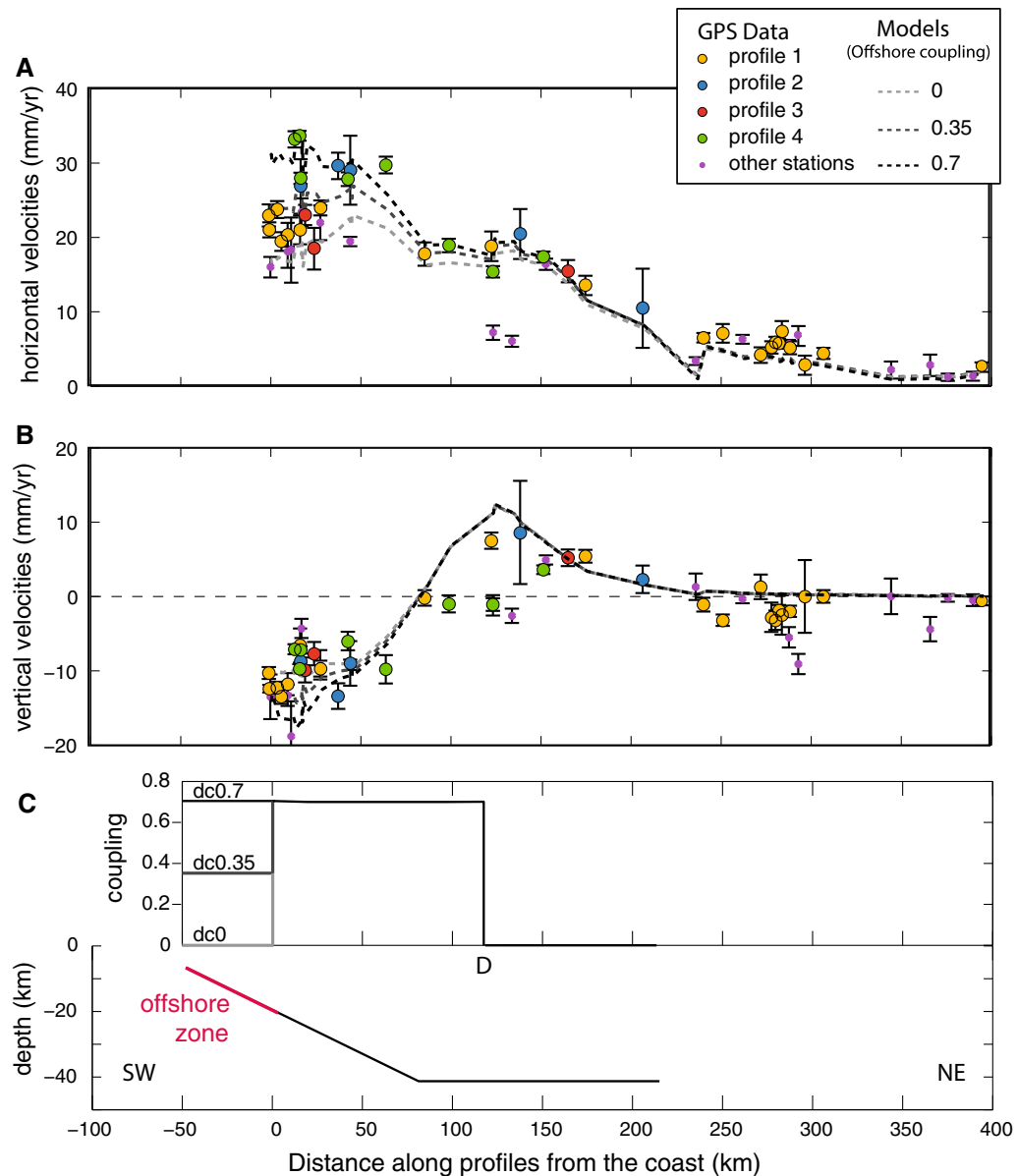
Figure 2

Trench-perpendicular profiles of the *horizontal* **a** and *vertical* **b** components of the 54 GPS site velocities used in this study and illustrated in Fig. 1. The *coloured dots* correspond to the groups of stations defined in Fig. 1. *Grey dashed lines* show three forward models with coupling values between the coast and trench of 0 (*light grey*), 0.35 (*mid grey*), and 0.7 (*black*). Velocities shown for those models are computed on GPS sites. **c** Forward modelling parameters along Profiles 1 to 4. The *top panel* shows the tested coupling values and the *bottom panel* shows a profile of the chosen fault plane geometry. Note that the lateral extension of these two planes is the same as the one used for static inversions in Fig. 3a. Offshore coupling values are set to 0, 0.35, or 0.7, as colour coded in **a**. The coupling from the coast inland to distance D is set to 0.7 and drops to 0 beyond point D

variations in the coupling offshore, a topic that we focus on in later sections (Fig. 2). To relate the slip on a given patch of the subduction interface to the surface displacements, we build Green's functions following the discrete wave number method (Bou-chon 1981, 2003) in an elastic stratified medium, assuming the Hernandez *et al.* (2001) velocity model and using AXITRA software (Coutant 1989).

The geometry of the subduction interface that we adopt for the forward modelling is similar to Geometry B from RADIGUET et al. (2012). The interface consists of two planar segments, one that initiates at the trench and dips 15° to the northeast and the other continuing inland beneath the continent at a horizontal angle (Fig. 2c). This geometry is referred to as the 2D flat-ramp geometry in the following. A discussion about the effect of the slab geometry on the coupling is made in Sect. 3.3. We constrain the rake angle to be 80° everywhere along the subduction interface, representing the best compromise rake angle found by RADIGUET et al. (2012) for the inter-SSE period.

The vertical component of inter-SSE velocities is sensitive to the location and depth of the transition between partially coupled and steadily slipping areas of the subduction interface (e.g. KANDA and SIMONS 2012). Simple forward models in which we varied both the coupling and distance D from the trench to the coupled–uncoupled transition best fit the GPS site velocities for a transition that is ~ 175 km from the trench (See supplementary materials for details).
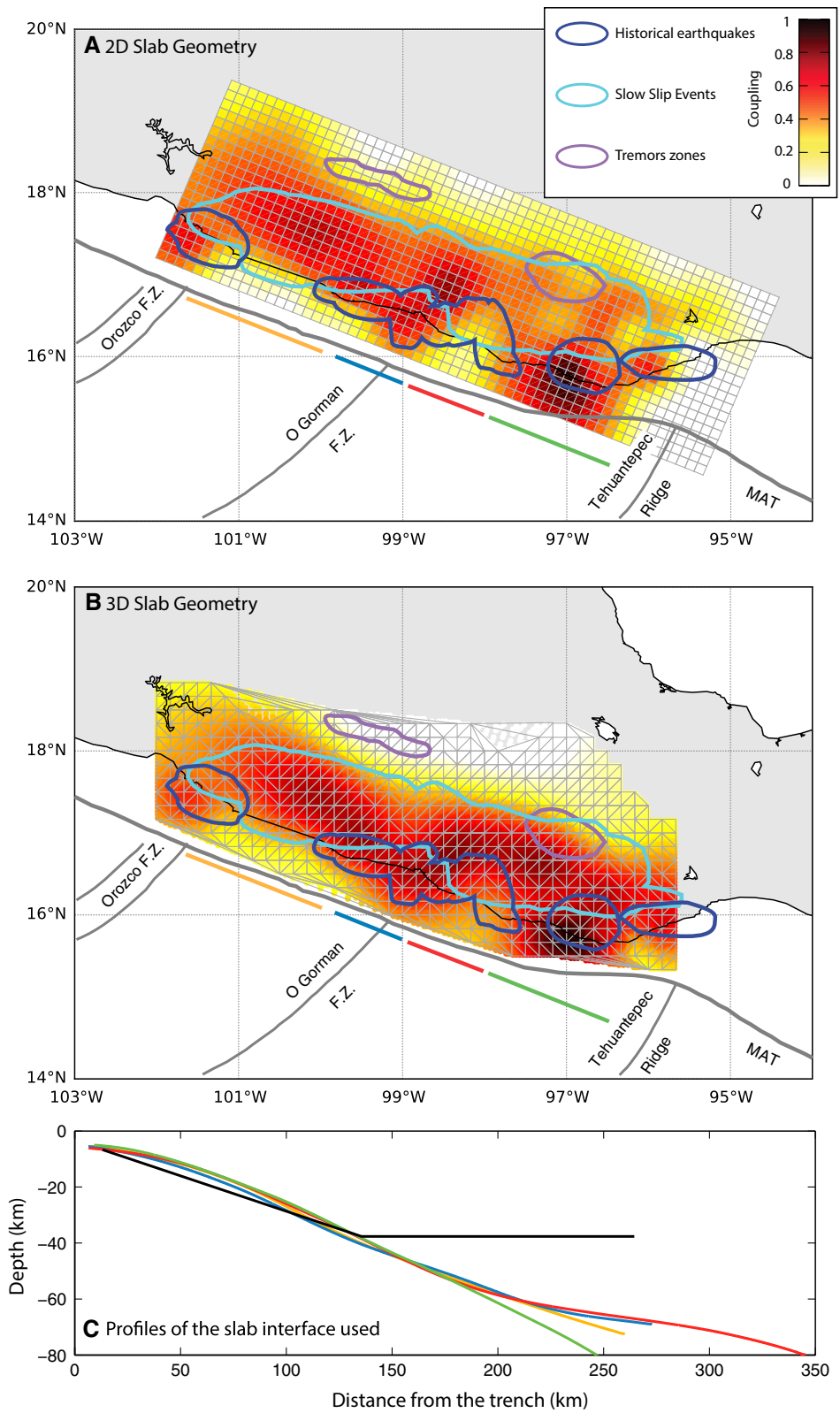
We also use elastic forward modelling to evaluate whether the differences between the site velocities that are predicted for average coupling values of 0, 0.35, and 0.7 along the shallowest (offshore) part of the subduction interface are large enough to be resolved by GPS measurements at coastal and near-coastal sites. Each model applies uniform interface coupling of 0.7 between the coast and distance D (175 km) (Fig. 2c). The elastic velocities that are predicted by these three forward models span the range of the observed velocities (Fig. 2), suggesting that to first order, coupling coefficients between 0 and 0.7 are necessary to fit the horizontal velocities and, to a lesser degree, the observed vertical rates. Stations along Profiles 2 and 4 (in orange and purple in Fig. 2) are best matched for shallow coupling values of 0.35 to 0.7, whereas stations along Profiles 1 and 3 (in yellow and red in Fig. 2) are best matched by coupling values smaller than 0.35. We conclude that, despite the parameter cross-correlation not investigated in those forward models, significant variations in coupling across the shallowest part of the subduction interface are detectable with the GPS velocities that are available for this study.

3.3. Static Inversions

While forward models highlight first-order characteristics of the coupling distribution, static inversions provide a more precise view of its spatial variations. Following the approach of RADIGUET et al. (2012), we use the least square formulation for linear problems (TARANTOLA 2005) to invert the 3D GPS velocities for the optimal 2D distribution of coupling along the subduction interface (Fig. 3a, b). The geometry of the Mexican subduction interface, imaged over the Guerrero area by the Meso-America Subduction Experiment (MASE) (KIM et al. 2012), reveals a flat subduction interface at ~ 40 km depth and ~ 100 km from the trench. But the lateral extension of this flat interface is not known. The recent Slab1.0 (HAYES et al. 2012) model based on a large compilation from earthquake catalogues to active seismology profiles and bathymetry presents a 3D geometry for the whole subduction zone. This geometry is well constrained at depths below 20 km and interpolated at larger depths with few constraints from deep earthquakes. It is not well constrained at intermediate depths and is not consistent with the geometry derived from receiver functions analysis in the Guerrero area (Fig. 3c). To assess the effect of the slab interface geometry on our coupling results, we test two different geometries: the 2D flat-ramp geometry presented in the forward approach and compatible with receiver functions analysis and the 3D interface of HAYES et al. (2012) (Fig. 3c). Note that both are consistent at shallow depths offshore, where the Slab1.0 geometry shows very little

Figure 3 ▶

Best-fit inter-SSE coupling solutions for 2 slab geometries from our GPS site velocities inversion. **a** Best coupling solution for a uniform ramp-flat slab geometry. **b** Best coupling solution for the 3D Slab1.0 geometry from HAYES et al. (2012). The four *bold coloured lines* along trench coincide with the four GPS station groups that are defined in Fig. 1. Contours of historical earthquakes, GPS-recorded slow slip events and tremor activity are in *dark blue* (SONG et al. 2009), *light blue* (RADIGUET et al. 2012; BRUDZINSKI et al. 2007; GRAHAM et al. 2014a) and *purple* (BRUDZINSKI et al. 2010), respectively. Notable offshore bathymetric features are shown (*F.Z.* Fracture zone, *MAT* Middle America Trench). **c** Slab geometry profiles used in models **a** and **b**. The *black* profile shows the flat-ramp 2D geometry used in model **a**, while the four colour profiles show the 3D geometry used in model **b** (profiles correspond to the central section of *boxes* in Fig. 1, with same colour code)

A 2D Slab Geometry

Legend:
- Historical earthquakes
- Slow Slip Events
- Tremors zones

Coupling scale: 0 to 1

B 3D Slab Geometry

C Profiles of the slab interface used
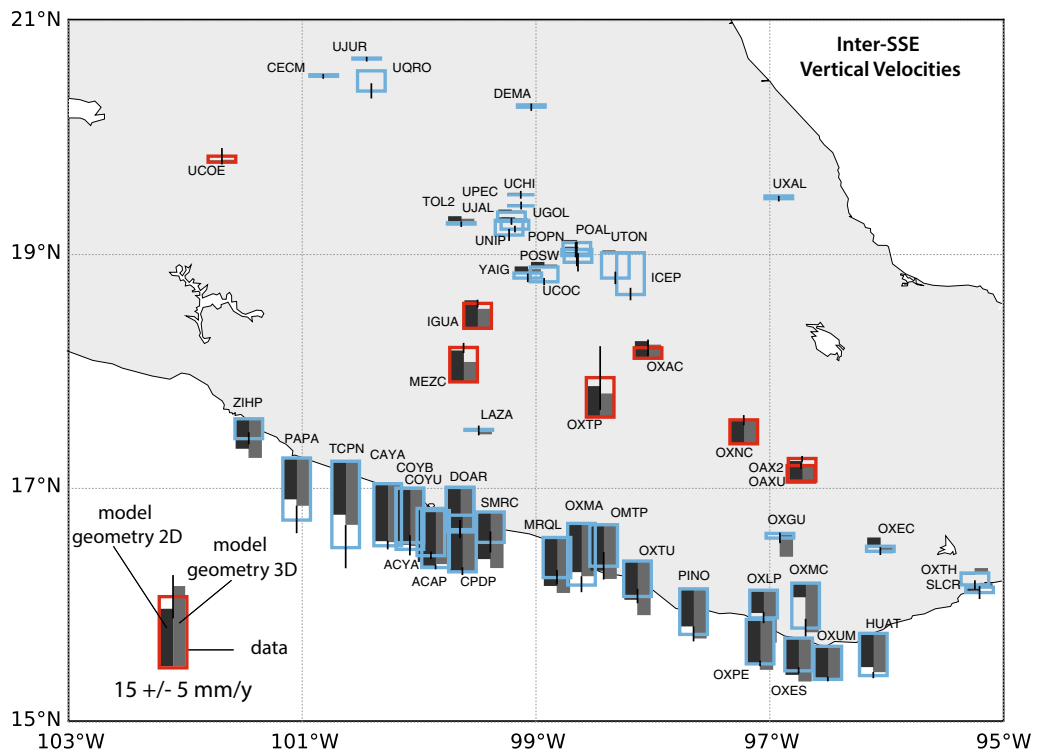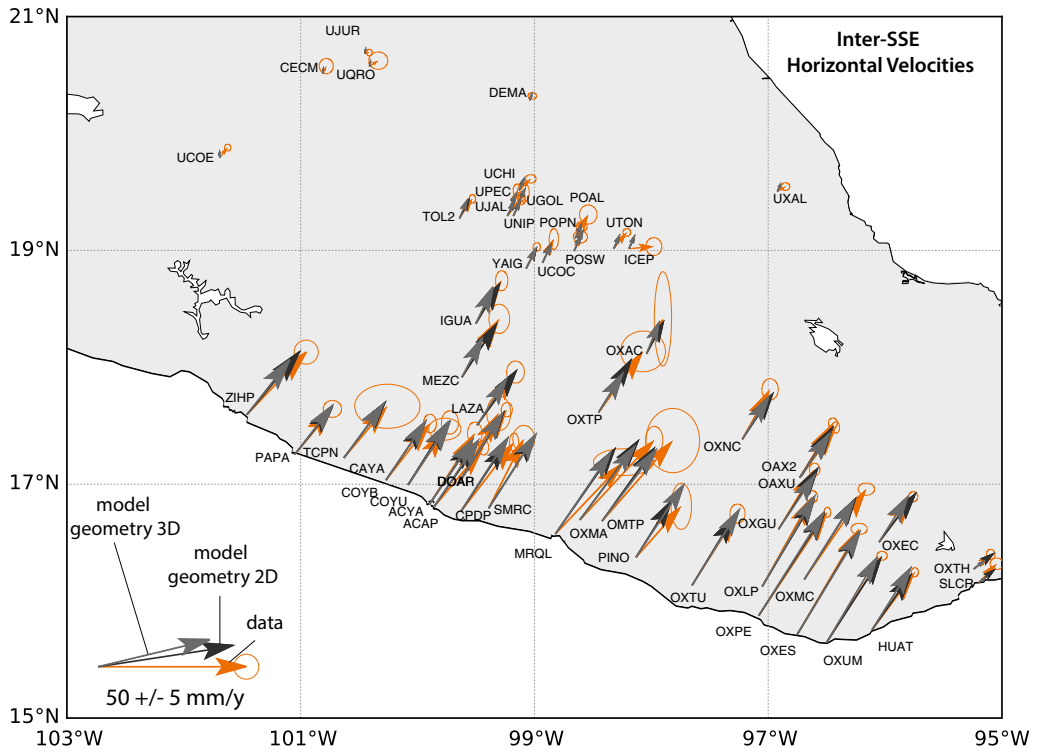
◄   Figure 4
Comparison of observed horizontal (*top*) and vertical (*bottom*)
inter-SSE GPS velocities to those predicted by best-fitting coupling
solutions shown in the previous figure. *Top Orange* and *grey*
vectors show the observed and predicted horizontal velocities,
respectively. *Light grey* corresponds to the 3D slab geometry
solution while *dark grey* corresponds to the 2D one. *Bottom Red*
and *blue boxes* show the observed uplift and subsidence rates,
respectively. Errors on vertical rates are shown by a fine *black line*
on *top of each box*. As for horizontal rates, *light grey boxes*
correspond to the 3D slab geometry solution while *dark grey boxes*
                     correspond to the 2D one

variations in dip angle along strike. The precise
configuration and resolution of the inversion are
detailed in supplementary materials.

Preferred coupling solutions are shown in Fig. 3a,
b together with the location of SSEs, tremors and
historical earthquakes. The horizontal and vertical
components of the observed GPS velocities are well fit
by both models (Fig. 4) except for stations in Mexico
City that are subsiding due to non-tectonic ground
water extraction and compaction of lake sediments, as
documented by InSAR (LÓPEZ-QUIROZ *et al.* 2009).
The estimated coupling values are relatively homoge-
neous at intermediate depths of the slab, but vary along
strike at shallow depths. The location of the transition
between deeper, uncoupled areas of the subduction
interface and partly-to-fully coupled shallow areas is
consistent with that found by forward models, at
$\sim$ 175 km from the trench. The shallowest part of the
subduction interface consists of three strongly cou-
pled and two weakly coupled areas (Fig. 3),
consistent with our forward modelling results
(Fig. 2). The westernmost strongly coupled area,
however, is constrained by only one GPS station
velocity and is thus less reliably determined (also see
the resolution analysis presented in the supplemen-
tary materials). The two geometries tested show only
slight differences. The coupling is more important at
intermediate depths in Oaxaca with the 3D geometry
and the downdip transition between highly coupled
and fully uncoupled areas is sharpest with the 3D
geometry due to its higher dip angle at depth.

Slow slip events occur below $\sim$ 10 km depth in
partially coupled areas (<0.6), slightly overlapping at
places with historical earthquakes areas (Fig. 3). As
SSEs are located only below the continent, the
interseismic coupling distribution, sum of the inter-

SSE coupling and SSEs contributions, still presents
offshore coupling variations [GRAHAM *et al.* 2015,
(Figure 11)], on which we focus on in the following.
The most strongly coupled area in southern Mexico is
off the coast of Oaxaca, where finite element mod-
elling of inter-SSE velocities from a dense, mixed-
mode GPS network (CORREA-MORA *et al.* 2008) pre-
viously demonstrated that the most strongly coupled
part of the subduction interface coincides with the
rupture area of the 1978 M_w 7.6 earthquake (STEWART
et al. 1981). The area is therefore of high seismic
hazard. Tremor activity located on the inland/deepest
part of the flat slab coincides with low coupling (<0.3),
presumably because the interface is silently sliding
during the inter-SSE period.

4. *Relation Between Short-Term Coupling and Long-*
Term Morphology

Inter-SSE surface deformation depends on varia-
tions of slip at depth that we model as lateral variations
of coupling on the subduction interface. Earthquakes
and SSEs induce surface displacements in the opposite
direction as does inter-SSE, elastic shortening and
release accumulated elastic strain. In the case of an
homogeneous elastic medium, earthquakes and other
phenomena that accommodate slip along the subduction
interface release all of the accumulated elastic strain
(SAVAGE 1983). No long-term surface deformation such
as topography is thus created. Conversely, observations
of surface morphology along subduction zones (coastal
shape, crustal faults) show that lateral variations of these
features coincide with geodetically derived coupling
patterns at depth in some cases (e.g. BÉJAR-PIZARRO
et al. 2013), indicating that some interseismic or inter-
SSE deformation may be non-reversible.

Along the Mexican Subduction Zone, we compare
the shape of the coastline with the distribution of inter-
SSE coupling as modelled in the previous section. We
compute distances between the trench and the coast in
the direction of convergence, using the ETOPO1 Digital
Elevation Model (DEM) at $1'$ resolution (AMANTE and
EAKINS 2009) for the offshore part, combined with the
SRTM DEM at 90 m resolution (FARR *et al.* 2007) for
the inland part. Figure 5a compares the trench-to-coast
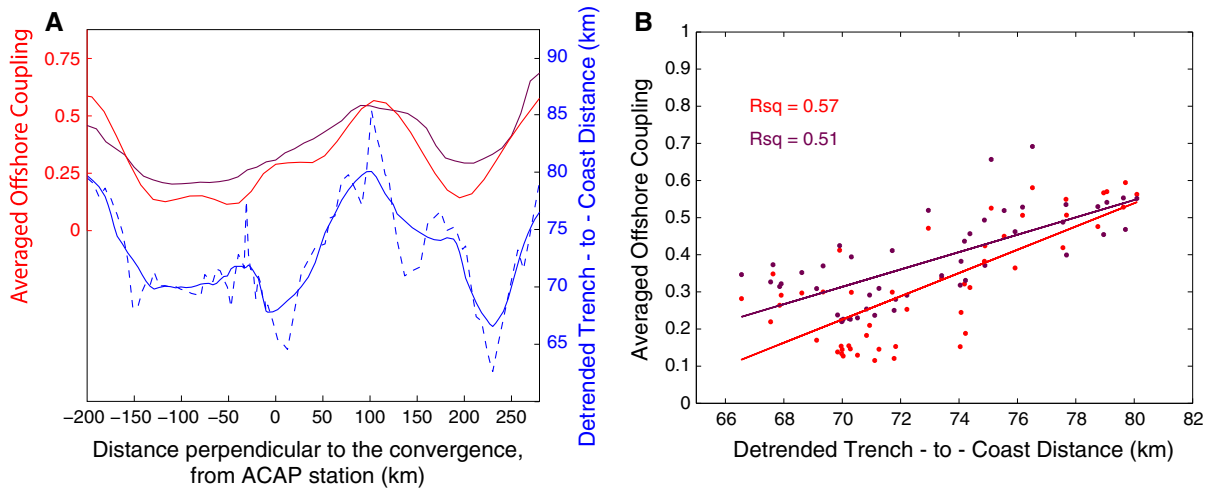distances corrected from a linear trend with lateral

Figure 5

Comparison of the GPS-derived offshore coupling (*red* 2D slab geometry solution, burgundy: 3D slab geometry solution) with trench-to-coast distances estimated along profiles parallel to the convergence direction (*blue*). **a** The along-strike, offshore coupling is computed by averaging coupling values between the trench and the coast in the convergence direction. The trench-to-coast distance is detrended and shown at full resolution (*dashed line*) and after smoothing with a 40 km sliding window (*plain line*). **b** Correlation plots between averaged offshore coupling and trench-to-coast distances (*red* 2D slab geometry solution, burgundy: 3D slab geometry solution). Linear regression coefficients are indicated for both linear regressions

variations of coupling below the accretionary prism between the trench and the coast. The noteworthy correlation for long wavelengths shows that weakly coupled areas coincide with lesser trench-to-coast distances while strongly coupled areas correspond to greater trench-to-coast distances. The linear regression coefficients between trench-coast distances and offshore coupling values are on the order of 0.5 for both geometries used in the coupling modelling (Fig. 5b). The correlation between the coastal shape and lateral coupling variations may be evidence for a mechanical relation between slip on the subduction interface and long-term surface deformation. To test this hypothesis and explore potential mechanisms involved, we use an independent analysis based on the mechanics of the accretionary wedge to determine the relationships between the long-term deformation of the forearc, its frictional properties and the coupling pattern.

5. Contribution of the Critical Taper Theory

Coulomb wedge theory (DAVIS *et al.* 1983) relates the mechanics of a 2D wedge submitted to a constant force applied on the backstop to the morphology of the

wedge and its internal mechanical parameters. To preserve the static stress equilibrium, the wedge evolves into a critical geometry for which every point of the wedge is on the verge of failure (i.e. the Mohr circle is tangent to the Coulomb failure envelope on a normal stress versus shear stress diagram) which means that the wedge undergoes internal deformation while sliding. For the critical state, the stress in the wedge can be explained by ψ_b, the angle between the maximum principal stress axis and the bottom of the wedge (Fig. 6a), and ψ_t, the angle between the maximum principal stress axis and the top of the wedge. ψ_b is a function of the basal friction angle ϕ_b and the internal Hubbert–Rubey pore pressure ratio λ, as defined in CUBAS *et al.* (2013b), and ψ_t depends on the internal friction angle ϕ_{int} and λ. We consider that the pore pressure is the same in the bulk of the wedge and on the bottom interface. Frictional angles ϕ are related to the friction μ by $\mu = \tan\phi$ and to the effective friction by $\mu^{\mathrm{eff}} = \tan\phi^{\mathrm{eff}} = (1 - \lambda)\tan\phi$. DAHLEN (1984) and LEHNER (1986) derived the constitutive relation that holds for the stress equilibrium of the wedge, the Coulomb yielding and the frictional sliding along the basal interface. This relation links ψ_b, ψ_t, the topographic slope α and the basement slope β (Fig. 6a):
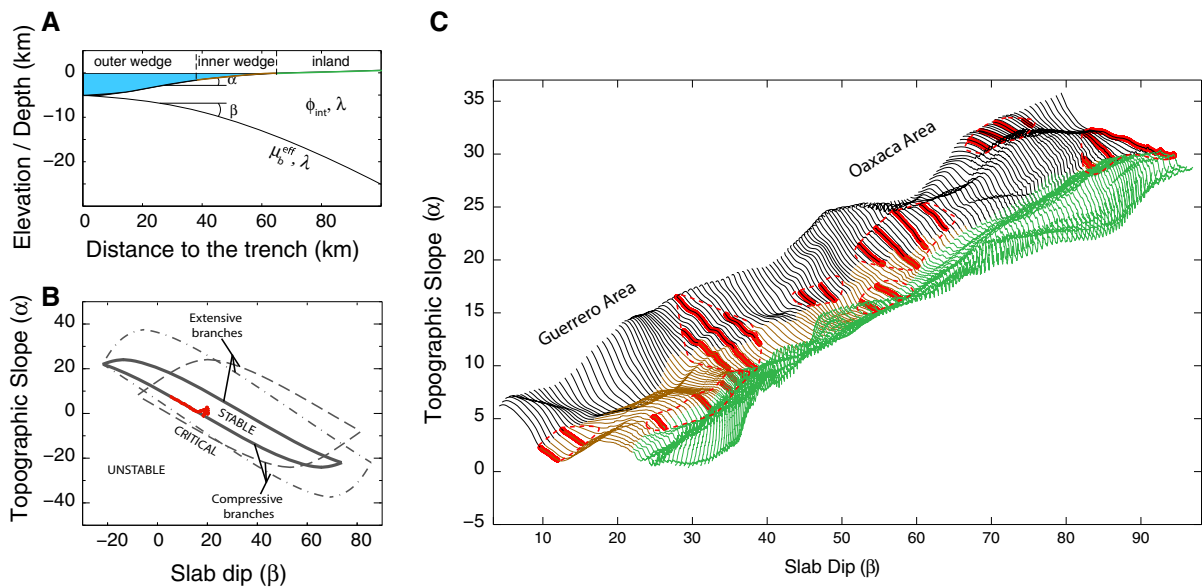
Figure 6

a Vertical cross section of the accretionary prism/upper plate that shows the model parameters used in critical taper theory (DAHLEN 1984). α and β are topographic and slab slopes, respectively. μ_b^{eff}, λ and ϕ_{int} are the effective friction on the subduction interface, the Hubbert–Rubey pore pressure and the internal friction angle, mechanical parameters considered in this study. *Black, orange and green lines* show the extents of the outer wedge, inner wedge and inland areas that are plotted in **c**. **b** Topographic slope as a function of slab dip derived from Dahlen's model for three various sets of mechanical properties (*continuous line* $\mu_b^{eff} = 0.25$, $\lambda = 0.65$; *dashed line* $\mu_b^{eff} = 0.09$, $\lambda = 0.65$; *pointed-dashed line* $\mu_b^{eff} = 0.25$, $\lambda = 0.40$). Stable, unstable and critical domains are shown. *Red line* is for profile of **a**. **c** Topographic slope as a function of slab dip for the 146, two-hundred-km-long trench-perpendicular profiles used for our study (see text for details). Each profile is shifted along *X* and *Y* axes from the previous one, by 0.2° and 0.5°, respectively (the bottom left profile is not shifted). *Red bold lines* identify the sections of the profiles that satisfy the conditions necessary for critical state areas. *Dashed red lines* contour critical state areas, where the mechanical parameters should be relatively uniform. Colours refer to location along profile as defined in **a**

$$\alpha + \beta = \psi_b - \psi_t \qquad (1)$$

Thus, given measurements of α and β, we can estimate the mechanical parameters of the wedge for morphologies consistent with critical state wedge conditions. For (α, β) couples located inside the critical enveloppe, the wedge is defined as being at stable state (Fig. 6b), which means that sliding can occur along the subduction interface without internal deformation.

Critical taper theory was first used to estimate average mechanical parameters for sub-aerial wedges such as Taiwan and submarine wedges (DAVIS *et al.* 1983; DAHLEN 1984; LALLEMAND *et al.* 1994). With improvements in resolution of the topography and slab geometry, CUBAS *et al.* (2013a, b) used the co-variation of α and β to retrieve mechanical properties along subduction zones and their spatial variations.

Here, we apply the method developed by CUBAS *et al.* (2013b) to the Mexican subduction forearc. We

use the 1-min resolution ETOPO1 DEM (AMANTE and EAKINS 2009) to compute the topographic slope α. We estimate the basement megathrust slope β from the slab geometry model Slab1.0 (HAYES *et al.* 2012), also used for the coupling static inversion. Figure 6a displays α versus β for 146 two-hundred-km-long serial profiles perpendicular to the trench, where the slab geometry is well constrained. At distances greater than 200-km inland from the trench, the lack of micro-seismicity on the flat part of the slab, which is otherwise well described by receiver functions analysis (PÉREZ-CAMPOS *et al.* 2008; KIM *et al.* 2012), prevents an accurate determination of lateral variations of the slab geometry. We manually selected critical state segments for all 146 α versus β profiles. In the Mexico subduction zone, where β ranges from 0° to 20°, compressive branches of Dahlen's model correspond to straight lines with negative slopes. Thus, finding a critical state segment in our data consists in finding linear trends that match
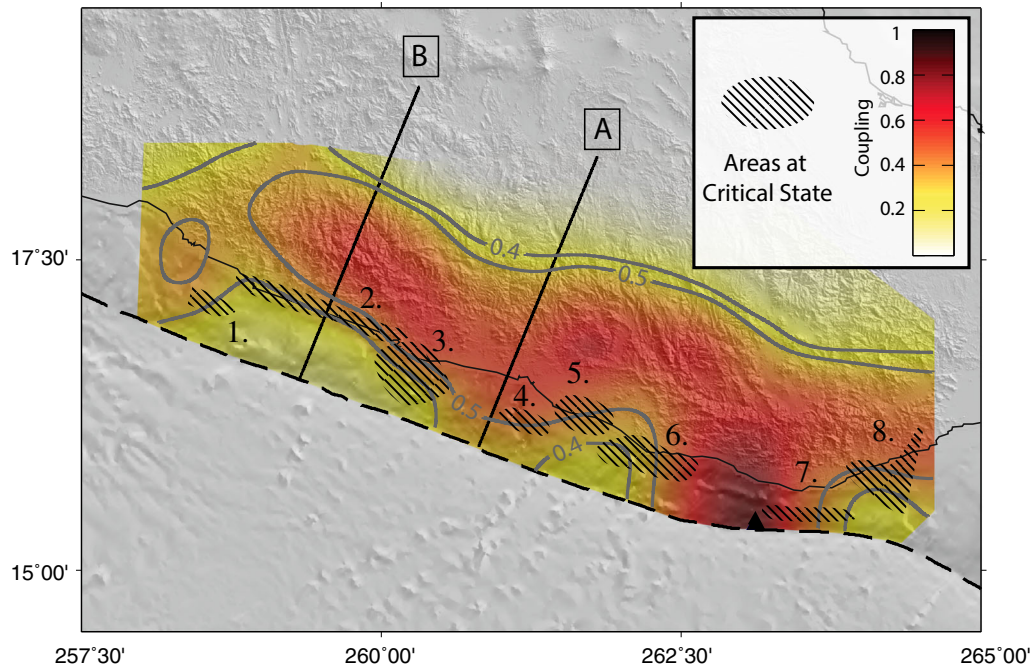
Figure 7

Overlay of the 8 critical state areas from Fig. 6 (*black stripes*) on the best-fitting coupling solution of Fig. 3b (3D slab geometry). Contours corresponding to transitional coupling values of 0.4 and 0.5 are shown by the *grey lines*. The two *black lines* show the location of Profiles **a** and **b** used for plastic deformation modelling (see Fig. 9)

Table 1

Best estimates of mechanical parameters for the eight critical state areas described in the text and identified in Fig. 7

Critical state areas	1.	2.	3.	4.	5.	6.	7.	8.
μ_b^{eff}	0.13	0.46	0.20	0.29	0.09	0.32	0.13	0.13
λ	0.67	0.47	0.78	0.45	0.73	0.58	0.68	0.73
μ_{int}	0.60	0.85	0.98	0.63	0.48	0.87	0.45	0.48

straight lines of Dahlen's model (Fig. 6b). After finding critical state segments in all profiles, we define 3D critical state areas by contouring compatible neighbours critical state segments (Figs. 6c, 7). The eight critical state areas that we identified are either narrow and elongated along the trench or are wider and extend from the trench to the coast, at morphological transitions. Critical state zones are all located at the transition between coupled and uncoupled areas, following a coupling contour of ~ 0.4–0.5.

To get a validation for the criticality of these areas as well as an estimate of their mechanical parameters μ_b^{eff}, λ and μ_{int}, we compute a misfit function for all critical state segments that we minimise following a L2 norm. Results are shown in Table 1. To evaluate

the robustness of the estimated parameters, we compute the probability density distribution of the model parameters and integrate it over one parameter to get 2D marginal probabilities. We compute them for each critical state segment on all profiles and average them to get the probability for a given critical state area (Fig. 8). The marginal probabilities are consistent between all eight critical state areas. Within 1σ, the ϕ_{int} probabilities range from 20° to 45°, the λ probabilities indicate that the parameter is poorly constrained, from 0.4 to 0.8, and ϕ_b^{eff} is better constrained and ranges from 3° to 25° depending on the critical area that is evaluated. The best fits for ϕ_{int} all lie within the 1σ contour, between 25° and 45° ($\mu_{\text{int}} = 0.47$ to 1). These agree with laboratory
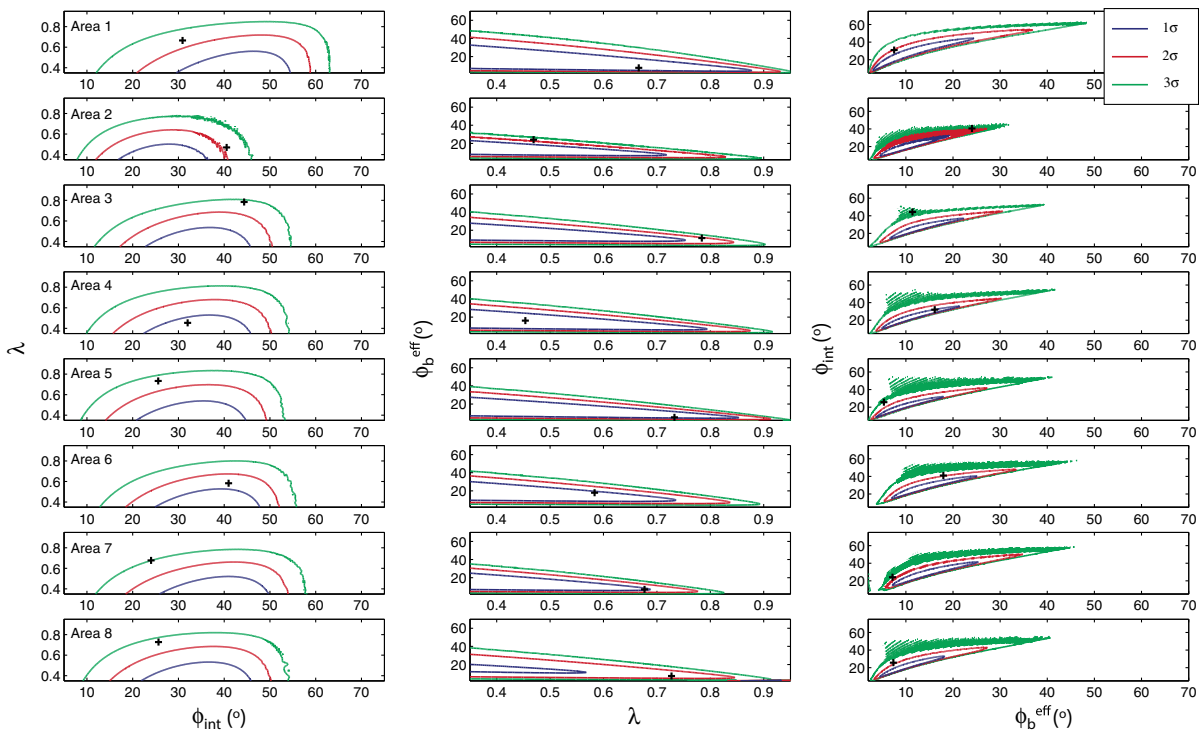
Figure 8

Marginal 2D probability distributions for all eight critical state areas. The three parameters estimated are λ: the Hubbert–Rubey pore fluid ratio, ϕ_b^{eff}: the effective basal friction angle and ϕ_{int}: the internal friction angle. The 1σ, 2σ and 3σ probability contours are shown in *blue, red and green*. The best fit is localised by a *black cross*

measurements of quartzo-feldspathic materials, which find internal frictions from 0.6 to 0.85 (BYER-LEE 1978). Though poorly constrained, the best fits for λ include values that are close to the hydrostatic pore fluid pressure ($\lambda = 0.4$). Best fits for ϕ_b^{eff} show significant lateral variations, with most values for ϕ_b^{eff} between 6° and 17° ($\mu_b^{\text{eff}} = 0.1$ to 0.3). ϕ_b^{eff} peaks at 25° ($\mu_b^{\text{eff}} = 0.46$) in critical area 2, which corresponds to the Guerrero seismic gap.

Applying critical taper theory to the Mexican subduction wedge thus reveals lateral variations of mechanical properties, with some parts of the wedge in the critical state, i.e. with internal deformation. The basal frictions are mainly low excepted in the Guerrero critical state area (area 2) that shows higher basal friction, in agreement with the presence of SSEs in this area. The long-term morphology of the Mexican margin might thus be driven by spatial variations of friction properties on the subduction interface, with critical state areas marking frictional transitions.

6. Discussion

In this study, we describe the Mexican subduction wedge with two models that describe deformation at different, but complementary timescales. Inter-SSE coupling (Sect. 3), which is a proxy for strain accumulating in the upper plate, operates over decadal time scales and varies significantly along strike. The morphological approach based on the critical taper theory (Sect. 5) describes average mechanical properties of the wedge on timescales that span several hundred seismic cycles (millennia or longer). The latter model enables to identify stable-state parts of the wedge, with no internal deformation, and critical state areas, where internal wedge deformation is likely to occur. All eight areas that we identified as critical state coincide with transitions between weakly coupled and strongly coupled areas of the subduction interface. This may indicate a persistency of mechanical properties through time, as is also

suggested by the correlation between the trench-to-coast distance and lateral coupling variations (Sect. 4).

None of the above invoke particular physical mechanisms to describe the dynamics of the deformation that leads to the present-day wedge morphology. In much of the following discussion, we explore the possible influence of plastic deformation on the observed morphology, beginning with an examination of whether some inter-SSE elastic strain may be homogeneously transferred into plastic upper plate deformation and continuing with an evaluation of the possible influence of frictional transitions along the subduction interface, using values derived from the critical taper model, on localisation of plastic deformation and morphological evolution of the wedge. Our discussion concludes with a description of two end-member and one intermediate set of mechanical wedge conditions that encompass a broad range of relations between interface coupling and surface morphologies observed along subduction zones.

6.1. Distributed Transfer of Elastic Inter-SSE Strain into Plastic Deformation of the Accretionary Prism

One hypothesis to explain the correspondence between the present-day pattern of inter-SSE coupling in southern Mexico and the long-term coastline morphology is that inter-SSE strain that accumulates due to partial-to-full locking of the subduction interface is not completely released by slip along the interface, including coseismic rupture, postseismic fault afterslip, and SSE. A fraction of the strain may instead be transferred into non-reversible, plastic deformation of the upper plate (LE PICHON *et al.* 1998). Horizontal inter-SSE velocities at locations near and along the coast are ~ 3 times faster than vertical rates, as illustrated by forward models (Fig. 2). By implication, if long-term plastic deformation mimics the pattern of what inferred elastic inter-SSE deformation models, the trench-to-coast distance is more sensitive to the horizontal than vertical components of the elastic deformation (and its variations along the trench). A simple calculation can be made to estimate the minimum time required to give rise to the observed

~ 20 km variations in the trench-to-coast distance for the Guerrero and Oaxaca segments (Fig. 5) if we simplistically assume that all of the present-day elastic inter-SSE strain is transferred into homogeneous plastic deformation of the upper plate. Given that the observed horizontal inter-SSE velocities vary along the trench by $\sim 15 \, \text{mm year}^{-1} \, (15 \, \text{km Myr}^{-1})$ (Fig. 2), a minimum of 1.3 Myr would be required to give rise to 20-km variations in the trench-to-coast distances. LE PICHON *et al.* (1998) instead suggest that only 5 % of the elastic deformation is transferred to plastic upper plate deformation in the case of the Japanese subduction zone. If so, to 27 Myr would be required to give rise to the 20-km trench-to-coast distance variations observed in southern Mexico. The millions of years that are required to shape the upper plate morphology is comparable to estimates made by BÉJAR-PIZARRO *et al.* (2013) for the Chilean subduction zone from a kilometre-scale correlation between a coastal scarp and the location of the transitional zone between coupled and uncoupled areas.

6.2. Localised Strain Transfer Associated with Frictional Transitions

An alternative scenario for permanently deforming the upper plate is if plastic, upper plate deformation occurs during sliding episodes (coseismic or aseismic slip) in response to variations of mechanical properties on the slab interface or within the wedge and overriding plate. Such variations could be of geological or geometrical origin as discussed before. With no direct information on sub-surface geological and geometrical structures in our study area, our considerations are indirect, based on the results from the critical taper analysis. To quantify how frictional transitions might produce brittle deformation during slip episodes, as already explored by other studies (e.g. HU and WANG 2008), we ran a mechanical model based on the limit analysis method (CHANDRASEKHARAIAH and DEBNATH 1994; SALENÇON 2002). The limit analysis method is a static approach that predicts the localisation of brittle deformation from the frictional properties distribution. It is based on the weak formulation of the force equilibrium (the principle of virtual powers) and the theorem of maximum rock strength (MAILLOT and LEROY 2006).

Table 2

Frictional parameters used in plastic deformation models HM and TM

Model	ϕ_{int} (°)	μ_{int}	λ	$\phi_{b,hdf}^{eff}$ (°)	$\mu_{b,hdf}^{eff}$	$\phi_{b,ldf}^{eff}$ (°)	$\mu_{b,ldf}^{eff}$
HM	35	0.7	0.4	NA	NA	5.7	0.1
TM	35	0.7	0.4	20	0.4	5.7	0.1

HM (Homogeneous Model) and TM (Transitional Model) are representative of profiles A and B in Fig. 7, respectively. Indices ldf and hdf refer to low dynamic friction and high dynamic friction, respectively

For our simulations, the Coulomb criterion is used to define the maximum rock strength. The simulations were run using the Optum-Geo software (OPTUMGEO 2013). Two different setups were investigated. The first one assumes that the subduction interface is homogeneously, strongly coupled, representative of Profile A in Fig. 7. Below, we refer to this as Model HM (Homogeneous Model). For the second, representative of Profile B in Fig. 7, we assume that the shallowest area of the subduction interface is uncoupled and then transitions downdip to a region of strong coupling coinciding with the critical state area we identified (Area 2 in Fig. 7). We refer below to this as Model TM (Transitional Model). We use the 2D slab geometry for these models.

The mechanical properties assumed for each model (Table 2) are consistent with those estimated for the eight critical state areas identified earlier in the analysis. We distinguish effective frictions for aseismic sliding and seismic sliding, corresponding to weakly coupled areas and strongly coupled areas, respectively. For aseismic areas, the effective friction of the slab interface is constrained by critical taper results: we use the friction obtained within a critical area near the transition zone, and extrapolate it to the whole aseismic area at shallower depths. It corresponds to a quasi-static friction since the slip is very slow. For seismic areas, since deformation is assumed to be acquired during sliding episodes, we use dynamic friction values consistent with values found for other subduction earthquakes (e.g. KIMURA *et al.* 2012; CONIN *et al.* 2012; FULTON *et al.* 2013; UJIIE *et al.* 2013; CUBAS *et al.* 2013a, b). Exact values for quasi-static or dynamic friction are not well constrained, but the important point is that dynamic friction is always way lower than quasi-static friction (e.g. RICE 2006; TORO *et al.* 2011).

We first plot the shear dissipation (Fig. 9), showing areas where the wedge is on the verge of brittle failure. In the HM model, a hinge associated with the transfer of material from the horizontal to the steeper portion of the slab is developed. Models that assume progressively more gradual slope transitions predict progressively more diffuse shear zones. In the TM model, a back-thrust develops at the frictional transition in addition to the slab kink hinge. Since the basal effective friction is larger along the uncoupled, shallow area of the subduction interface than along the more strongly coupled interface farther downdip, the frontal part of the wedge is uplifted along the predicted back-thrust. Increasing the frictional value that is imposed along the strongly coupled area of the interface increases the dip angle of the back-thrust.

The limit analysis approach provides virtual velocities on all nodes of the model. To retrieve surface displacements, we assume that the ratio between virtual velocities of two segments projected along their fault is equal to the ratio of actual displacements between those segments. All surface displacements are normalised to the surface horizontal displacement at the backstop. In that case, considering 1 m of displacement at the backstop, i.e. for 1 m of convergence, the forearc is uplifted by 63 cm in the TM model and 27 cm in the HM model (top panel Fig. 9). Those uplifts should obviously be balanced by erosion which is not quantified here. However, considering an homogeneous erosion rate along the coast, the larger uplift built in the TM model in comparison with the HM model would contribute to reduce the trench-to-coast distance, which is consistent with the observations made in Fig. 5. Contrary to the first scenario presented in Sect. 6.1, the coastal shape is there mostly built from differential vertical displacements (differences in
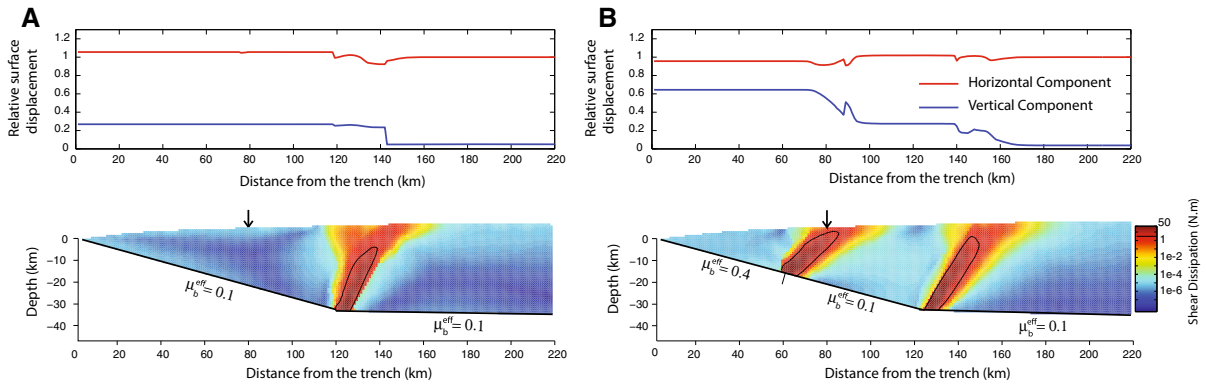
Figure 9
Deformation predicted by plastic modelling for two mechanical settings. Virtual displacement and virtual shear dissipation are obtained from limit analysis (OptumGeo 2013). **a** Is for a uniform low effective dynamic friction of 0.1 on the megathrust interface, while **b** is for an effective friction of 0.4 near the trench and a lower effective dynamic friction of 0.1 at depth. The density is set to 2600 kg/m^3. Slab geometry is identical as that used for the coupling modelling. Topography in **a** and **b** corresponds to that along Profiles **a** and **b** of Fig. 7. *Top panels* show the cumulative surface displacement due to brittle deformation (*red horizontal*, *blue vertical*) relative to the horizontal displacement at the backstop. *Bottom panels* represent the final shear dissipation in a logarithmic colourscale. The *black line* corresponds to the 5 N.m contour in which more than 99 % of the shear dissipation occurs. *Black arrows* indicate the location of the coastline
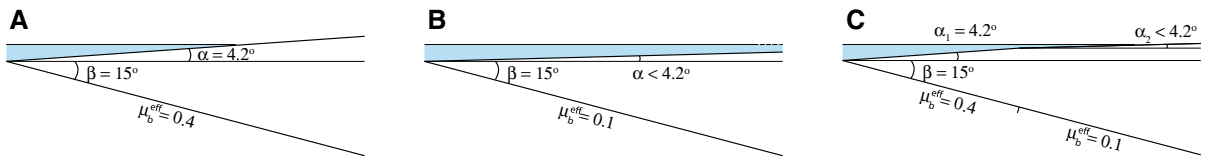

Figure 10
Sketches showing the influence of the effective basal friction μ_b^{eff} on the average topographic slope α. Other parameters are set constant ($\beta = 15°$, $\phi_{int} = 35°$, $\lambda = 0.4$). Cases **b** and **c** are similar to models **a** and **b** in Fig. 9

horizontal displacements between models TM and HM are very small, top panel Fig. 9).

Although homogeneous, upper plate plastic deformation that is proportional to the elastic strain accumulation (Sect. 6.1) and localised upper plate deformation due to frictional transitions on the subduction interface (Sect. 6.2) may both contribute to shaping coastlines, too few observational constraints are available to estimate their relative proportion, such as seismic profiles to identify splay faults which would attest of internal deformation in the prism.

6.3. Coastal Morphology as a Function of Frictional Variations Along Fault Dip

The evidence described above and shown in Fig. 5a for an along-strike correlation between areas of weak coupling on the shallow subduction interface

and diminished trench-to-coast distances agrees with a similar correlation described for other subduction zones, particularly in the eastern Pacific. Weakly coupled trench segments often coincide with prominent peninsulas (and hence very short trench-to-coast distances) such as the Arauco Peninsula in Chile (Melnick *et al.* 2009) and the Piura peninsula in northern Peru (Nocquet *et al.* 2014). Based on this correlation, we propose to distinguish three types of behaviours along subduction zones depending on how frictional properties vary downdip along the subduction interface (Fig. 10).

The first corresponds to subduction interfaces where coupling is weak between the trench and the downdip limit of the seismogenic zone (Fig. 10a). In this case, critical wedge theory predicts that the average topographic slope angle is high (4.2° for $\beta = 15°$ and $\mu_b^{eff} = 0.4$) and continual thickening of

the upper plate (wedge), possibly including forethrust sequences. These processes favour the genesis of peninsulas and decrease trench-to-coast distances.

The second corresponds to a strongly coupled slab interface from the trench to the downdip limit of the seismogenic zone (Fig. 10b and Profile A of Fig. 7), as assumed for the HM model described in Sect. 6.2. In this case, the entire subduction interface may rupture at very low dynamic friction. This results in low average topographic slope angles ($<4.2°$ for $\beta = 15°$ and $\mu_b^{\text{eff}} = 0.1$), including negative slope angles that may be associated with extension of the forearc and the formation of sedimentary basins. Sedimentary basins in forearc settings have been detected by their free-air gravity anomalies and are spatially correlated with large seismic asperities that broke during the 20th century (WELLS *et al.* 2003; SONG and SIMONS 2003). Larger trench-to-coast distances are expected in this scenario.

The intermediate case consists of a subduction interface with frictional transitions within the seismogenic zone (Fig. 10c and Profile B of Fig. 7), as described for the TM model of Sect. 6.2. These frictional transitions may produce localised upper plate deformation, that may result in different topographic slope angles for the outer and inner wedges. The resultant trench-to-coast distance is intermediate between that expected for the two end-member scenarios described above.

subduction wedge. Using critical taper theory to relate the morphology of the subduction wedge to its average long-term mechanical properties, we identify eight critical state areas where internal deformation of the wedge is expected. All eight are located at transitions between weakly and strongly coupled areas of the subduction interface. An inversion of mechanical parameters for these critical state areas gives values that are consistent for 7 of the 8 critical state areas, with the lone exception coinciding with the Guerrero seismic gap, where anomalously high basal friction estimated from our inversion overlaps the region where silent slip events occur. Two mechanisms are proposed to explain how trench-to-coast distances have evolved to their present geometry in southern Mexico: (1) homogeneous plastic deformation of the upper plate may occur in response to inter-SSE elastic strain associated with the locked subduction interface (over time scales of Myrs), (2) frictional transitions on the subduction interface may produce localised shear zones in the upper plate and may cause differential uplift and/or subsidence along-strike in the upper plate. Our results suggest that the geometry/morphology of the subduction wedge can be related to its long-term mechanical parameters. To address in further detail how permanent deformation accumulates over one seismic cycle, dynamic modelling that incorporates rupture mechanics processes and of fault deformation could be appropriate.

7. Conclusion

Our analysis of the inter-SSE velocities of continuous GPS sites in southern Mexico reveals that significant variations in inter-SSE coupling occur along the Oaxaca and Guerrero segments of the Mexico subduction zone. The along-strike variations, alternating between areas where coupling is less than 0.3 and areas where it is more than 0.7, are mostly offshore. Coupling at depths below 25 km is more homogeneous and transitions to steady creep at distances of ~ 175 km from the trench. Variations in shallow coupling along the trench are strongly correlated with trench-to-coast distances, the latter of which may be a proxy for the mechanical state of the

constructive criticism which we found very helpful to improve the manuscript.

REFERENCES

AMANTE, C. and EAKINS, B. W. (2009). *ETOPO1 1 arc-minute global relief model: procedures, data sources and analysis.* US Department of Commerce, National Oceanic and Atmospheric Administration, National Environmental Satellite, Data, and Information Service, National Geophysical Data Center, Marine Geology and Geophysics Division.

ASTIZ, L. and KANAMORI, H. (1984). *An earthquake doublet in ometepec, guerrero, mexico.* Physics of the earth and planetary interiors, 34(1):24–45.

BÉJAR-PIZARRO, M., SOCQUET, A., ARMIJO, R., CARRIZO, D., GENRICH, J., and SIMONS, M. (2013). *Andean structural control on interseismic coupling in the north chile subduction zone.* Nature Geoscience.

BEKAERT, D., HOOPER, A., and WRIGHT, T. (2015). *A spatially-variable power-law tropospheric correction technique for insar data.* Journal of Geophysical Research: Solid Earth.

BOUCHON, M. (1981). *A simple method to calculate green's functions for elastic layered media.* Bulletin of the Seismological Society of America, 71(4):959–971.

BOUCHON, M. (2003). *A review of the discrete wavenumber method.* Pure and applied Geophysics, 160(3-4):445–465.

BRUDZINSKI, M., CABRAL-CANO, E., CORREA-MORA, F., DEMETS, C., and MÁRQUEZ-AZÚA, B. (2007). *Slow slip transients along the oaxaca subduction segment from 1993 to 2007.* Geophysical Journal International, 171(2):523–538.

BRUDZINSKI, M. R., HINOJOSA-PRIETO, H. R., SCHLANSER, K. M., CABRAL-CANO, E., ARCINIEGA-CEBALLOS, A., DIAZ-MOLINA, O., and DEMETS, C. (2010). *Nonvolcanic tremor along the oaxaca segment of the middle america subduction zone.* Journal of Geophysical Research, 115(null):B00A23.

BÜRGMANN, R., KOGAN, M. G., STEBLOV, G. M., HILLEY, G., LEVIN, V. E., and APEL, E. (2005). *Interseismic coupling and asperity distribution along the kamchatka subduction zone.* Journal of Geophysical Research: Solid Earth (1978-2012), 110(B7).

BYERLEE, J. (1978). *Friction of rocks.* Pure and applied Geophysics, 116(4-5):615–626.

CAVALIÉ, O., PATHIER, E., RADIGUET, M., VERGNOLLE, M., COTTE, N., WALPERSDORF, A., KOSTOGLODOV, V., and COTTON, F. (2013). *Slow slip event in the mexican subduction zone: Evidence of shallower slip in the guerrero seismic gap for the 2006 event revealed by the joint inversion of insar and gps data.* Earth and Planetary Science Letters, 367:52–60.

CHANDRASEKHARAIAH, D. and DEBNATH, L. (1994). *Continuum mechanics.* Academic press New York.

CHLIEH, M., AVOUAC, J.-P., SIEH, K., NATAWIDJAJA, D. H., and GALETZKA, J. (2008). *Heterogeneous coupling of the sumatran megathrust constrained by geodetic and paleogeodetic measurements.* Journal of Geophysical Research: Solid Earth (1978–2012), 113(B5).

CHLIEH, M., MOTHES, P., NOCQUET, J.-M., JARRIN, P., CHARVIS, P., CISNEROS, D., FONT, Y., COLLOT, J.-Y., VILLEGAS-LANZA, J.-C., ROLANDONE, F., et al. (2014). *Distribution of discrete seismic asperities and aseismic slip along the ecuadorian megathrust.* Earth and Planetary Science Letters, 400:292–301.

CHLIEH, M., PERFETTINI, H., TAVERA, H., AVOUAC, J.-P., REMY, D., NOCQUET, J.-M., ROLANDONE, F., BONDOUX, F., GABALDA, G., and BONVALOT, S. (2011). *Interseismic coupling and seismic potential along the central andes subduction zone.* Journal of Geophysical Research: Solid Earth (1978–2012), 116(B12).

CONIN, M., HENRY, P., GODARD, V., and BOURLANGE, S. (2012). *Splay fault slip in a subduction margin, a new model of evolution.* Earth and Planetary Science Letters, 341:170–175.

CORREA-MORA, F., DEMETS, C., CABRAL-CANO, E., DIAZ-MOLINA, O., and MARQUEZ-AZUA, B. (2009). *Transient deformation in southern mexico in 2006 and 2007: Evidence for distinct deep-slip patches beneath guerrero and oaxaca.* Geochemistry, Geophysics, Geosystems, 10(2).

CORREA-MORA, F., DEMETS, C., CABRAL-CANO, E., MARQUEZ-AZUA, B., and DIAZ-MOLINA, O. (2008). *Interplate coupling and transient slip along the subduction interface beneath oaxaca, mexico.* Geophysical Journal International, 175(1):269–290.

COTTE, N., WALPERSDORF, A., KOSTOGLODOV, V., VERGNOLLE, M., SANTIAGO, J.-A., and CAMPILLO, M. (2009). *Anticipating the next large silent earthquake in mexico.* Eos, Transactions American Geophysical Union, 90(21):181–182.

COUTANT, O. (1989). *Programme de simulation numerique axitra. Rapport LGIT.*

CUBAS, N., AVOUAC, J., LEROY, Y., and PONS, A. (2013a). *Low friction along the high slip patch of the 2011 mw 9.0 tohoku-oki earthquake required from the wedge structure and extensional splay faults.* Geophysical Research Letters, 40(16):4231–4237.

CUBAS, N., AVOUAC, J.-P., SOULOUMIAC, P., and LEROY, Y. (2013b). *megathrust friction determined from mechanical analysis of the forearc in the maule earthquake area.* Earth and Planetary Science Letters.

CUBAS, N., LAPUSTA, N., AVOUAC, J.-P., and PERFETTINI, H. (2015). *Numerical modeling of long-term earthquake sequences on the ne japan megathrust: comparison with observations and implications for fault friction.* Earth and Planetary Science Letters, 419:187–198.

DAHLEN, F. (1984). *Noncohesive critical coulomb wedges: An exact solution.* Journal of Geophysical Research: Solid Earth (1978–2012), 89(B12):10125–10133.

DAVIS, D., SUPPE, J., and DAHLEN, F. (1983). *Mechanics of fold-and-thrust belts and accretionary wedges.* Journal of Geophysical Research: Solid Earth (1978–2012), 88(B2):1153–1172.

DEMETS, C., GORDON, R. G., and ARGUS, D. F. (2010). *Geologically current plate motions.* Geophysical Journal International, 181(1):1–80.

DI TORO, G., HAN, R., HIROSE, T., DE PAOLA, N., NIELSEN, S., MIZOGUCHI, K., FERRI, F., COCCO, M., and SHIMAMOTO, T. (2011). *Fault lubrication during earthquakes.* Nature, 471(7339):494–498.

FARR, T. G., ROSEN, P. A., CARO, E., CRIPPEN, R., DUREN, R., HENSLEY, S., KOBRICK, M., PALLER, M., RODRIGUEZ, E., ROTH, L., et al. (2007). *The shuttle radar topography mission.* Reviews of geophysics, 45(2).

FRANCO, A., LASSERRE, C., LYON-CAEN, H., KOSTOGLODOV, V., MOLINA, E., GUZMAN-SPEZIALE, M., MONTEROSSO, D., ROBLES, V., FIGUEROA, C., AMAYA, W., et al. (2012). *Fault kinematics in northern central america and coupling along the subduction interface of the cocos plate, from gps data in chiapas (mexico), guatemala and el salvador.* Geophysical Journal International, 189(3):1223–1236.

FRANK, W. B., RADIGUET, M., ROUSSET, B., SHAPIRO, N. M., HUSKER, A. L., KOSTOGLODOV, V., COTTE, N., and CAMPILLO, M. (2015).

Uncovering the geodetic signature of silent slip through repeating earthquakes. Geophysical Research Letters, *42*(8):2774–2779.

FRANK, W. B., SHAPIRO, N. M., KOSTOGLODOV, V., HUSKER, A. L., PAYERO, J. S., CAMPILLO, M., and PRIETO, G. A. (2013). *Low-frequency earthquakes in the mexican sweet 1 spot*. Geophysical Research Letters.

FULTON, P., BRODSKY, E., KANO, Y., MORI, J., CHESTER, F., ISHIKAWA, T., HARRIS, R., LIN, W., EGUCHI, N., TOCZKO, S., et al. (2013). *Low coseismic friction on the tohoku-oki fault determined from temperature measurements*. Science, *342*(6163):1214–1217.

GRAHAM, S. E., DEMETS, C., CABRAL-CANO, E., KOSTOGLODOV, V., ROUSSET, B., WALPERSDORF, A., COTTE, N., LASSERRE, C., MCCAFFREY, R., and SALAZAR-TLACZANI, L. (2015). *Slow slip history for the mexico subduction zone: 2005 through 2011*. Pure and Applied Geophysics.

GRAHAM, S. E., DEMETS, C., CABRAL-CANO, E., KOSTOGLODOV, V., WALPERSDORF, A., COTTE, N., BRUDZINSKI, M., MCCAFFREY, R., and SALAZAR-TLACZANI, L. (2014a). *Gps constraints on the 2011-2012 oaxaca slow slip event that preceded the 2012 march 20 ometepec earthquake, southern mexico*. Geophysical Journal International, page ggu019.

GRAHAM, S. E., DEMETS, C., CABRAL-CANO, E., KOSTOGLODOV, V., WALPERSDORF, A., COTTE, N., BRUDZINSKI, M., MCCAFFREY, R., and SALAZAR-TLACZANI, L. (2014b). *Gps constraints on the mw= 7.5 ometepec earthquake sequence, southern mexico: coseismic and post-seismic deformation*. Geophysical Journal International, *199*(1):200–218.

HAYES, G. P., WALD, D. J., and JOHNSON, R. L. (2012). *Slab1. 0: A three-dimensional model of global subduction zone geometries*. Journal of Geophysical Research: Solid Earth (1978–2012), *117*(B1).

HERNANDEZ, B., SHAPIRO, N., SINGH, S., PACHECO, J., COTTON, F., CAMPILLO, M., IGLESIAS, A., CRUZ, V., GÓMEZ, J., and ALCÁNTARA, L. (2001). *Rupture history of september 30, 1999 intraplate earthquake of oaxaca, mexico (mw= 7.5) from inversion of strong-motion data*. Geophysical research letters, *28*(2):363–366.

HU, Y. and WANG, K. (2008). *Coseismic strengthening of the shallow portion of the subduction fault and its effects on wedge taper*. Journal of Geophysical Research: Solid Earth (1978-2012), *113*(B12).

HUSKER, A. L., KOSTOGLODOV, V., CRUZ-ATIENZA, V. M., LEGRAND, D., SHAPIRO, N. M., PAYERO, J. S., CAMPILLO, M., and HUESCA-PÉREZ, E. (2012). *Temporal variations of non-volcanic tremor (nvt) locations in the mexican subduction zone: Finding the nvt sweet spot*. Geochemistry, Geophysics, Geosystems, *13*(3).

KANDA, R. V. and SIMONS, M. (2012). *Practical implications of the geometrical sensitivity of elastic dislocation models for field geologic surveys*. Tectonophysics.

KANEKO, Y., AVOUAC, J.-P., and LAPUSTA, N. (2010). *Towards inferring earthquake patterns from geodetic observations of interseismic coupling*. Nature Geoscience, *3*(5):363–369.

KIM, Y., MILLER, M. S., PEARCE, F., and CLAYTON, R. W. (2012). *Seismic imaging of the cocos plate subduction zone system in central mexico*. Geochemistry, Geophysics, Geosystems, *13*(7).

KIMURA, G., HINA, S., HAMADA, Y., KAMEDA, J., TSUJI, T., KINOSHITA, M., and YAMAGUCHI, A. (2012). *Runaway slip to the trench due to rupture of highly pressurized megathrust beneath the middle trench slope: the tsunamigenesis of the 2011 tohoku earthquake off the east coast of northern japan*. Earth and Planetary Science Letters, *339*:32–45.

KONCA, A. O., AVOUAC, J.-P., SLADEN, A., MELTZNER, A. J., SIEH, K., FANG, P., LI, Z., GALETZKA, J., GENRICH, J., CHLIEH, M., et al. (2008). *Partial rupture of a locked patch of the sumatra megathrust during the 2007 earthquake sequence*. Nature, *456*(7222):631–635.

KOSTOGLODOV, V., BANDY, W., DOMINGUEZ, J., and MENA, M. (1996). *Gravity and seismicity over the guerrero seismic gap, mexico*. Geophysical Research Letters, *23*(23):3385–3388.

KOSTOGLODOV, V., HUSKER, A., SHAPIRO, N. M., PAYERO, J. S., CAMPILLO, M., COTTE, N., and CLAYTON, R. (2010). *The 2006 slow slip event and nonvolcanic tremor in the mexican subduction zone*. Geophysical Research Letters, *37*(24).

LALLEMAND, S. E., SCHNÜRLE, P., and MALAVIEILLE, J. (1994). *Coulomb theory applied to accretionary and nonaccretionary wedges: Possible causes for tectonic erosion and/or frontal accretion*. Journal of Geophysical Research: Solid Earth (1978–2012), *99*(B6):12033–12055.

LAPUSTA, N., RICE, J. R., BEN-ZION, Y., and ZHENG, G. (2000). *Elastodynamic analysis for slow tectonic loading with spontaneous rupture episodes on faults with rate-and state-dependent friction*. Journal of Geophysical Research: Solid Earth (1978–2012), *105*(B10):23765–23789.

LE PICHON, X., MAZZOTTI, S., HENRY, P., and HASHIMOTO, M. (1998). *Deformation of the japanese islands and seismic coupling: an interpretation based on gsi permanent gps observations*. Geophysical Journal International, *134*(2):501–514.

LEHNER, F. (1986). *Comments on "noncohesive critical coulomb wedges: An exact solution" by fa dahlen*. Journal of Geophysical Research: Solid Earth (1978–2012), *91*(B1):793–796.

LIU, Y. and RICE, J. R. (2007). *Spontaneous and triggered aseismic deformation transients in a subduction fault model*. Journal of Geophysical Research: Solid Earth (1978–2012), *112*(B9).

LÓPEZ-QUIROZ, P., DOIN, M.-P., TUPIN, F., BRIOLE, P., and NICOLAS, J.-M. (2009). *Time series analysis of mexico city subsidence constrained by radar interferometry*. Journal of Applied Geophysics, *69*(1):1–15.

LOVELESS, J. P. and MEADE, B. J. (2011). *Spatial correlation of interseismic coupling and coseismic rupture extent of the 2011 mw= 9.0 tohoku-oki earthquake*. Geophysical Research Letters, *38*(17):L17306.

LOWRY, A. R., LARSON, K. M., KOSTOGLODOV, V., and BILHAM, R. (2001). *Transient fault slip in guerrero, southern mexico*. Geophysical Research Letters, *28*(19):3753–3756.

MAILLOT, B. and LEROY, Y. M. (2006). *Kink-fold onset and development based on the maximum strength theorem*. Journal of the Mechanics and Physics of Solids, *54*(10):2030–2059.

MARQUEZ-AZUA, B. and DEMETS, C. (2009). *Deformation of mexico from continuous gps from 1993 to 2008*. Geochemistry, Geophysics, Geosystems, *10*(2).

MAZZOTTI, S., LE PICHON, X., HENRY, P., and MIYAZAKI, S.-I. (2000). *Full interseismic locking of the nankai and japan-west kurile subduction zones: An analysis of uniform elastic strain accumulation in japan constrained by permanent gps*. Journal of Geophysical Research: Solid Earth (1978–2012), *105*(B6):13159–13177.

MELNICK, D., BOOKHAGEN, B., STRECKER, M. R., and ECHTLER, H. P. (2009). *Segmentation of megathrust rupture zones from fore-arc deformation patterns over hundreds to millions of years, arauco peninsula, chile*. Journal of Geophysical Research: Solid Earth (1978–2012), *114*(B1).

Metois, M., Socquet, A., and Vigny, C. (2012). *Interseismic coupling, segmentation and mechanical behavior of the central chile subduction zone*. Journal of Geophysical Research: Solid Earth (1978–2012), *117*(B3).

Nocquet, J., Villegas-Lanza, J., Chlieh, M., Mothes, P., Rolandone, F., Jarrin, P., Cisneros, D., Alvarado, A., Audin, L., Bondoux, F., et al. (2014). *Motion of continental slivers and creeping subduction in the northern andes*. Nature Geoscience, *7*(4):287–291.

OptumGeo (2013). Optum computational engineering. *http://www.optumce.com*.

Ortiz, M., Singh, S., Kostoglodov, V., and Pacheco, J. (2000). *Source areas of the acapulco-san marcos, mexico earthquakes of 1962 (m 7.1; 7.0) and 1957 (m 7.7), as constrained by tsunami and uplift records*. GEOFISICA INTERNACIONAL-MEXICO-, *39*(4):337–348.

Pérez-Campos, X., Kim, Y., Husker, A., Davis, P. M., Clayton, R. W., Iglesias, A., Pacheco, J. F., Singh, S. K., Manea, V. C., and Gurnis, M. (2008). *Horizontal subduction and truncation of the cocos plate beneath central mexico*. Geophysical Research Letters, *35*(18).

Radiguet, M., Cotton, F., Vergnolle, M., Campillo, M., Valette, B., Kostoglodov, V., and Cotte, N. (2011). *Spatial and temporal evolution of a long term slow slip event: the 2006 guerrero slow slip event*. Geophysical Journal International, *184*(2):816–828.

Radiguet, M., Cotton, F., Vergnolle, M., Campillo, M., Walpersdorf, A., Cotte, N., and Kostoglodov, V. (2012). *Slow slip events and strain accumulation in the guerrero gap, mexico*. Journal of Geophysical Research: Solid Earth (1978–2012), *117*(B4).

Rice, J. R. (2006). *Heating and weakening of faults during earthquake slip*. Journal of Geophysical Research: Solid Earth (1978–2012), *111*(B5).

Salençon, J. (2002). *De l'élasto-Plasticité au Calcul à la Rupture*. Editions Ecole Polytechnique.

Savage, J. (1983). *A dislocation model of strain accumulation and release at a subduction zone*. Journal of Geophysical Research: Solid Earth (1978–2012), *88*(B6):4984–4996.

Singh, S. C., Hananto, N., Mukti, M., Robinson, D. P., Das, S., Chauhan, A., Carton, H., Gratacos, B., Midnet, S.,

Djajadihardja, Y., et al. (2011). *Aseismic zone and earthquake segmentation associated with a deep subducted seamount in sumatra*. Nature Geoscience, *4*(5):308–311.

Song, T.-R. A., Helmberger, D. V., Brudzinski, M. R., Clayton, R. W., Davis, P., Pérez-Campos, X., and Singh, S. K. (2009). *Subducting slab ultra-slow velocity layer coincident with silent earthquakes in southern mexico*. Science, *324*(5926):502–506.

Song, T.-R. A. and Simons, M. (2003). *Large trench-parallel gravity variations predict seismogenic behavior in subduction zones*. Science, *301*(5633):630–633.

Stewart, G. S., Chael, E. P., and McNally, K. C. (1981). *The november 29, 1978, oaxaca, mexico, earthquake: A large simple event*. Journal of Geophysical Research: Solid Earth (1978–2012), *86*(B6):5053–5060.

Suárez, G. and Sánchez, O. (1996). *Shallow depth of seismogenic coupling in southern mexico: Implications for the maximum size of earthquakes in the subduction zone*. Physics of the earth and planetary interiors, *93*(1):53–61.

Tarantola, A. (2005). *Inverse problem theory and methods for model parameter estimation*. Society for Industrial & Applied.

Ujiie, K., Tanaka, H., Saito, T., Tsutsumi, A., Mori, J. J., Kameda, J., Brodsky, E. E., Chester, F. M., Eguchi, N., Toczko, S., et al. (2013). *Low coseismic shear stress on the tohoku-oki megathrust determined from laboratory experiments*. Science, *342*(6163):1211–1214.

Vergnolle, M., Walpersdorf, A., Kostoglodov, V., Tregoning, P., Santiago, J., Cotte, N., and Franco, S. (2010). *Slow slip events in mexico revised from the processing of 11 year gps observations*. Journal of Geophysical Research: Solid Earth (1978–2012), *115*(B8).

Walpersdorf, A., Cotte, N., Kostoglodov, V., Vergnolle, M., Radiguet, M., Santiago, J. A., and Campillo, M. (2011). *Two successive slow slip events evidenced in 2009–2010 by a dense gps network in guerrero, mexico*. Geophysical Research Letters, *38*(15).

Wells, R. E., Blakely, R. J., Sugiyama, Y., Scholl, D. W., and Dinterman, P. A. (2003). *Basin-centered asperities in great subduction zone earthquakes: A link between slip, subsidence, and subduction erosion?* Journal of Geophysical Research, *108*(B10):2507.